

# $^{56}\text{Fe}(\nu_e, e^-)^{56}\text{Co}$ : A Technique for an Accurate Cross Section Measurement at ORLaND

Yu.Efremenko

*Department of Physics and Astronomy, University of Tennessee,  
Knoxville, TN 37996,  
E-mail: efremenk@unix.utk.edu*

F.T.Avignone

*Department of Physics and Astronomy, University of South Carolina,  
Columbia, SC 29208,  
E-mail: waters@psc.psc.sc.edu*

A.Mezzacappa

*Physics Division, Oak Ridge National Laboratory,  
Oak Ridge, TN 37831,  
E-mail mezz@mail.phy.ornl.gov*

A detector design is presented that would allow the measurement of the cross section of  $^{56}\text{Fe}(\nu_e, e^-)^{56}\text{Co}$  with a statistical accuracy of a few % at the ORLaND facility at the SNS. Monte Carlo simulations are presented to document the detector response.

## 1 Motivation

Core collapse supernovae are stellar explosions disrupting almost entirely stars more massive than  $8 - 10 M_{\odot}$  and extremely important for Galactic dynamical and chemical evolution because of their energetics and nucleosynthesis. Neutrino–nucleus weak interactions play a central role in both supernova dynamics and supernova nucleosynthesis. These interactions are also central to existing and proposed terrestrial facilities to detect neutrinos from the next Galactic or near–extra-Galactic supernova, which in turn will provide detailed neutrino “lightcurves” from which supernova models and supernova nucleosynthesis models can be diagnosed and improved. Although many nuclei participate in these weak interactions and it is impossible to measure all of the relevant cross sections, measurement of a few key cross sections would provide invaluable checks on the elaborate theoretical models used to compute them<sup>1</sup>.

At the end of a massive star’s life, it’s core is composed of iron-group nuclei. This core is surrounded by layers of successively lighter elements, such as silicon, oxygen, carbon, helium, and hydrogen. The core becomes gravitationally unstable, collapses on itself, rebounds at supernuclear densities, and generates a shock wave that propagates out of the core, through the outer

layers, disrupting the star in a supernova. The stage is set, i.e., where the shock forms in the core and how much energy is imparted to it when it does form, by the “deleptonization” of the core during collapse. Deleptonization occurs via electron capture on iron-group nuclei and on free protons. Initially, the electron neutrinos produced escape the core, carrying away lepton number. However, as the core densities increase beyond  $10^{11}$  g/cm<sup>3</sup>, the electron neutrinos become trapped, and electron neutrino capture begins to compete with electron capture until, eventually, these two inverse weak interactions are equilibrated. At this point, the deleptonization “ceases” on the timescale of core collapse. Thus, one or two measurements of the cross sections for electron neutrino capture on iron-group nuclei (e.g.,  $\sigma[{}^{56}\text{Fe}(\nu_e, e^-){}^{56}\text{Co}]$ ) would provide important input to models of stellar core collapse and the post-core-bounce supernova evolution.

After the shock forms, the stellar core is stratified. Neutrinos of all flavors are radiating from a proto-neutron star at the center of the explosion at the staggering rate of  $10^{57}$  neutrinos per second and  $10^{45}$  Watts. The electron neutrinos and antineutrinos power the supernova via neutrino absorption on the dissociation-liberated nucleons behind the shock. All three flavors of neutrinos interact with nuclei in the outer stellar layers, via neutral- and charged-current reactions, producing nuclear transmutations that play an important role in supernova nucleosynthesis. In some cases, these neutrino–nucleus interactions provide the channels for the production of some of Nature’s rarest isotopes<sup>2</sup>. The same technique proposed to measure the neutrino–iron cross section can be used to measure the neutrino–nucleus cross section on any of the following nuclei:  ${}^7\text{Li}$ ,  ${}^9\text{Be}$ ,  ${}^{11}\text{B}$ ,  ${}^{27}\text{Al}$ ,  ${}^{40}\text{Ca}$ ,  ${}^{51}\text{V}$ ,  ${}^{52}\text{Cr}$ ,  ${}^{55}\text{Mn}$ ,  ${}^{59}\text{Co}$ ,  ${}^{93}\text{Nb}$ ,  ${}^{115}\text{In}$ ,  ${}^{181}\text{Ta}$ , and  ${}^{209}\text{Bi}$ .

Finally, iron is one of the materials proposed for the next-generation supernova neutrino detector, OMNIS, now in its planning stages<sup>3</sup>. Accurate measurements of both charged- and neutral-current neutrino–iron cross sections would be invaluable in its design and, ultimately, in the interpretation of its supernova neutrino data.

## 2 Theoretical Background

The first estimate of the neutrino-iron cross section was made by Bugaev<sup>4</sup> using the shell model. More recently, the inclusive cross section of  ${}^{56}\text{Fe}(\nu_e, e^-){}^{56}\text{Co}$ , averaged over the stopped muon decay neutrino spectrum, was calculated by Kolbe, Langanke, and Martinez-Pinedo<sup>5</sup>, and by Kolbe and Langanke<sup>6</sup>. In ref. <sup>6</sup>, the neutral current cross sections for the production of neutrinos and their spectra are presented for both Fe and Pb.

The charged-current neutrino-nucleus cross section between nuclear states with specific angular momenta and isospin was derived by Walecka <sup>7</sup>, and by Donnelly and Peccei <sup>8</sup>. This cross section involves a Gamow-Teller (GT) contribution and forbidden transitions. Random phase approximations (RPA) are not as reliable as shell model calculations for transitions mediated by the GT operator; however, they do describe forbidden transitions adequately <sup>5</sup>.

The shell model calculation of the GT contributions to the cross section  $^{56}\text{Fe}(\nu_e, e^-)^{56}\text{Co}$  of refs. 5 and 6 were performed within the complete pf-shell using the large-space Strasbourg-Madrid codes developed by Caurier <sup>9,10</sup>. The forbidden transitions were calculated with the RPA.

The resulting cross section, weighted by the neutrino spectrum from decay of a stopped muon, is  $2.64 \cdot 10^{-40} \text{cm}^2$ . The only measurement of this cross section was reported by the KARMEN collaboration [ $2.56 \pm 1.08(\text{stat}) \pm 0.43(\text{sys}) \cdot 10^{-40} \text{cm}^2$  <sup>11</sup>]. A much more accurate measurement is needed.

According to a computational feasibility study reported here, it can be measured with a statistical accuracy of a few percent with a high-granularity detector described below called SOUDANINO.

### 3 Feasibility Study of the Proposed Detector

The geometry and principle of operation of the SOUDANINO detector are similar in principle those of the Soudan-II detector, from which it gets its name <sup>12</sup>. It is composed of iron tubes with thin walls, each containing a position-sensitive gas tube; see Fig. 1. The signal would be read out separately from each individual tube. Particle energy is reconstructed by the range of the particle track or by the total number of fired cells. Directional information can be extracted from the reconstruction of the track. In principle, this detector can be constructed in such way that iron tubes will be replaceable. After making measurements with one set of "target" tubes, they might be replaced by the tubes made from a new material (new target). As a result, neutrino interactions with different nuclei can be studied with the same detector.

Detectors with gas tubes as the sensitive elements have a number of advantages compared, for example, to those with scintillator rods. In general, they are less expensive, and do not require a complex light-readout system. In addition, the low mass of this part of the detector eliminates the necessity to subtract interactions in the target from the interactions in the detector itself. The energy resolution for electrons in the energy range of a few tens of MeV is better by measurement of the track length than by measurement of total energy deposition.

The design of such a detector should be a reasonable compromise between

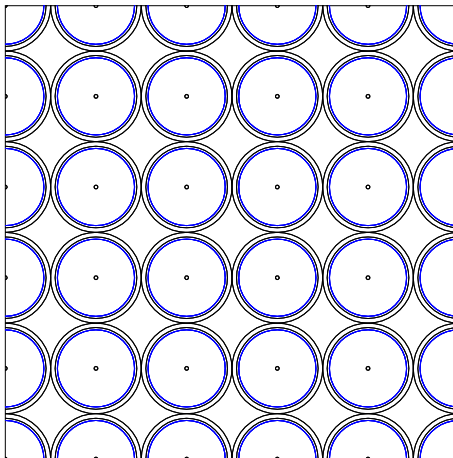


Figure 1: Schematic view of proposed SOUDANINO detector.

cost and performance. The thinner the tube walls, the better the energy and angular resolution. On the other hand, the thinner tube walls give the detector less average density and, as a result, increase the size and the number of channels. We obtained an initial optimization of the detector using a GEANT Monte Carlo code. As a result of this study, we conclude that the optimum iron wall thickness is 0.5 mm. The dimensions are OD = 10 mm and ID = 9 mm.

In the rate calculations, the detector was assumed to be at a distance of 50 m from the 2-megawatt target of the Spallation Neutron Source (SNS). For the theoretical cross section of  $2.64 \cdot 10^{-40} \text{ cm}^2$ , the neutrino flux at the detector of  $3 \cdot 10^6 \nu_e \text{ cm}^{-2} \text{ sec}^{-1}$ , and the number of iron atoms in one ton ( $9.9 \cdot 10^{27} \text{ ton}^{-1}$ ), the expected reaction rate is 250 events  $y^{-1} \text{ ton}^{-1}$ . We estimate a detection efficiency of 30%. For a desired reconstructed event rate of  $1000 y^{-1}$ , the active detector mass should be 13.3 tons, corresponding to a fiducial volume of  $2.5 \times 2.5 \times 2.5 \text{ m}^3$ . This fiducial part of the detector should be surrounded by at least 50 cm of active detector. As a result, the total detector size would be  $3.5 \times 3.5 \times 3.5 \text{ m}^3$  and would consist of a  $314 \times 314$  array of parallel tubes.

During the Monte Carlo study of the SOUDANINO performance we compared two types of active elements for the detector, scintillator rods, and gaseous drift tubes. The results of the simulation of SOUDANINO, for 30-MeV electrons for both gas tubes and scintillator rods, are shown in Fig. 2. For this simulation, an ideal light readout (no photo-electron statistical fluc-

tuations) was assumed. The energy resolution by measurement of the total energy is 21.4%; the energy resolution measured by track range is 23.4%. For the real detector, the first value will be worse because of the fluctuations in the light collection system. On the lower part of the figure, the simulation of the detector with gas tubes is shown. The average number of fired cells is less and resolution is slightly worse for gas tube detectors compared with scintillator, because of the lower efficiency to low-energy photons.

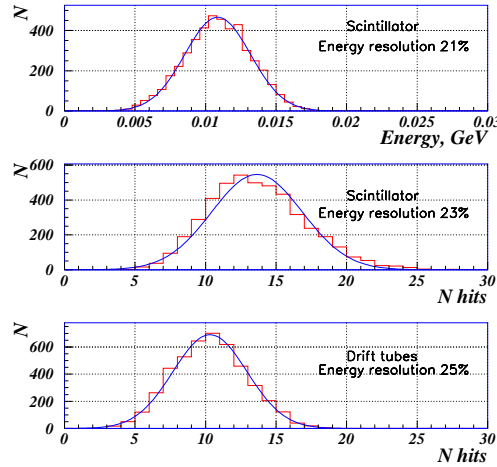


Figure 2: Detector energy resolution, with scintillator and gas drift tube sensitive volume. Energy reconstructed by total energy deposition (upper figure), by the number of fired cells for scintillator (middle figure), and by number of gas drift tubes (lower figure). The electron energy is 30 MeV.

For the energies of interest, the probability to start an electromagnetic shower is small; therefore, the measurement of the energy using the number of fired cells for electrons has excellent linearity as can be seen in Fig. 3.

For the iron detector with tubes 1 cm in diameter and walls 0.5 mm thick, the average density will be  $1.35 \text{ g cm}^{-3}$ . The 13.5-ton cubic detector will have a fiducial dimension of 2.5 meters on a side. With a fiducial cut of 0.5 meters around the entire detector, the total dimension should be  $3.5 \times 3.5 \times 3.5 \text{ m}^3$ . The number of tubes to be read out will be about  $10^5$ . The measurement of the energy by range does not require amplitude information from the tubes, and as a result, a relatively simple, inexpensive electronic system can be used. The results of simulations for this type of detector are presented in Fig. 4 where the

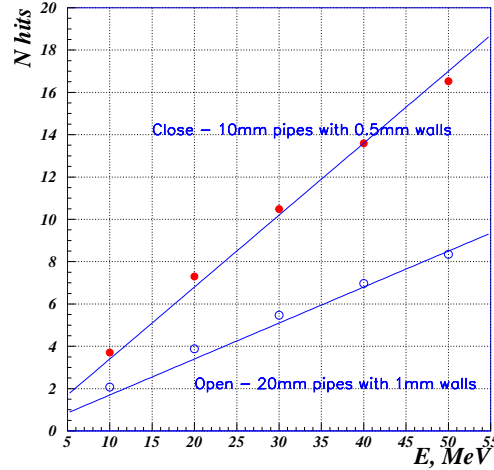


Figure 3: Linearity of the SOUDANINO detector for two different tube thickness for gas drift tubes.

energy and angular resolutions are presented. For electrons with an energy of 30 MeV, the predicted energy resolution will be 25% and the angular resolution is about  $15^\circ$ .

The major source of beam-correlated background will be interactions of high-energy neutrons produced in the SNS target and penetrating into the ORLaND facility. Their interaction might knock out a high-energy proton which could imitate the track of an electron. However, to fire the same number of cells as an electron, the proton should have a much higher energy, see Fig. 5. For example, a 140-MeV proton can produce the same number of hits as a 35-MeV electron. Already this energy-cut significantly reduces the contribution from this source of background. In addition, it is possible to separate electrons from protons with the same number of hits by the shape of the track. The proton tracks are more linear, and the electron tracks are irregular in shape because of the emission of photons. In Fig. 6, examples of the coordinates of firing cells, for 40-MeV electrons and 125-MeV protons are shown. By the introduction of the "track linearity parameter," which is the  $\chi^2$  of how well one can fit the track with a straight line, one can separate electrons from protons for a signal with the same number of hits. See Fig 7, and Fig 8. Of course, more sophisticated algorithms can produce better separation.

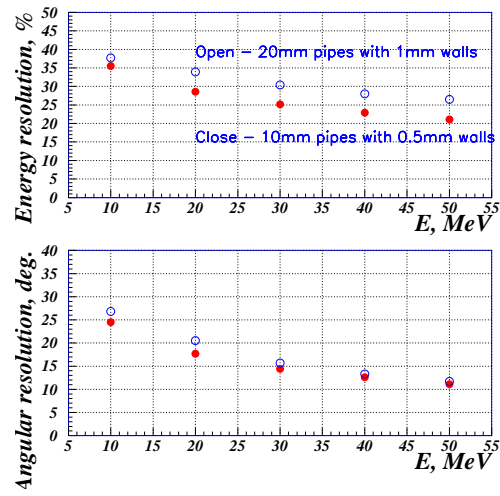


Figure 4: Energy and angular resolution for the the Soudanino detector for two different tube thicknesses.

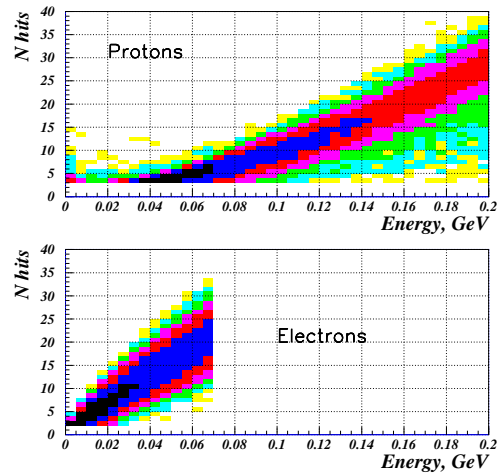


Figure 5: Detector response for protons and electrons.

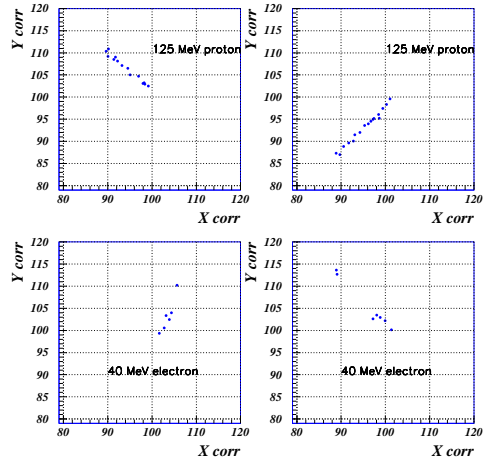


Figure 6: Sample track for 125-MeV proton and 40-MeV electron in the SOUDANINO detector.

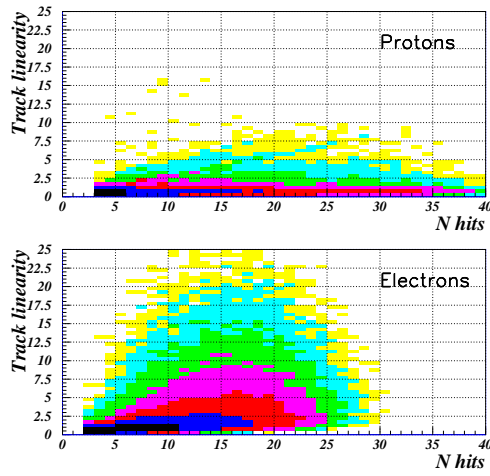


Figure 7: Track Linearity parameter for the protons and electrons in the detector.

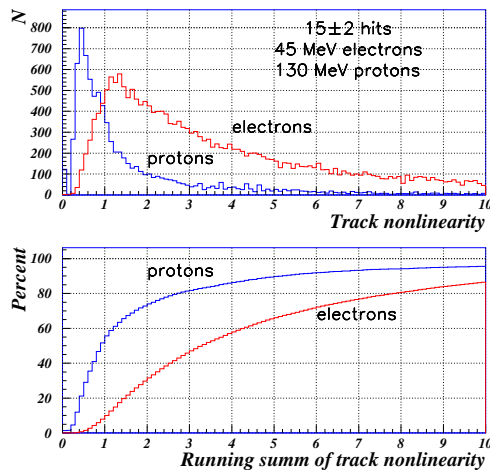


Figure 8: Rejection of the protons from the electrons by Track Linearity parameter.

## 4 Conclusions

We have investigated in detail the response of a highly segmented detector with a fiducial mass of 13.3 tons of iron-clad gas tube detectors. An accurate cross section of the reaction  $^{56}\text{Fe}(\nu_e, e^-)^{56}\text{Co}$  can be measured with such detector placed at 50 meters from the target station of the SNS (under construction at ORNL). Detailed Monte Carlo computations show that simple gas tube detectors with position sensitivity give an energy resolution comparable to scintillation detectors. This technique can be applied to any targets that can be fabricated into tubes of 1 cm OD, with thin walls and with lengths of 3.5 m. These measurements would yield  $\nu_e$ -nucleus cross section of great importance to neutrino astrophysics.

## 5 Acknowledgments

YuE is supported by the Oak Ridge National Laboratory and the University of Tennessee, FTA is supported by the U.S. DoE Office of High Energy Physics, and the University of South Carolina, AM is supported at the Oak Ridge National Laboratory, managed by UT-Battelle, LLC, for the U.S. Dept. of Energy under contract DE-AC05-00OR22725.

## References

1. E. Kolbe, and K.-H. Langanke, and G. Martinez-Pinedo, *Phys. Rev. C* **60**, 52801 (1999).
2. S. E. Woosley, and D. Hartmann, and R. D. Hoffman, and W. C. Haxton, *The Astrophysical Journal* **356**, 272 (1990).
3. D. B. Cline, *et al*, *Phys. Rev. D* **D50**, 720 (1994).
4. E. V. Bugaev et al., *Nucl. Instrum. Methods* **A324**, 350 (1979)
5. E. Kolbe, K. Langanke and G. Martinez-Pinedo, Preprint: arXiv:nucl-th/9905001 3 Aug, 1999.
6. E. Kolbe and K. Langanke, Preprint: arXiv:nucl-th/0003060 27 March 2000.
7. J. D. Walecka, in Muon Physics, eds. V. W. Hughes and C. S. Wu (Academic Press, New York, 1975) p.113.
8. T. W. Donnelly and R. D. Peccei, *Phys. Rep.* **50**, 1 (1979).
9. E. Caurier, computer code ANTOINE, CRN, Strasbourg, 1989
10. E. Caurier, G. Martinez-Pinedo, F. Nowacki, A. Poves, J. Retamosa and A. P. Zuker *Phys. Rev. C* **C59**, 2033 (1999)
11. K. Eitel, Private Communication, G. Ruf, diploma thesis, University of Bonn.
12. W.W.M. Allison, *Nucl. Instrum. Methods* **A376**, 36 (1996)